CHEMICAL PHYSICS

Relayed hyperpolarization for zero-field nuclear magnetic resonance

Erik T. Van Dyke[1,2,3], James Eills[1,2,3,4], Román Picazo-Frutos[1,2,3], Kirill F. Sheberstov[1,2,3,5], Yinan Hu[1,2,3], Dmitry Budker[1,2,3,6], Danila A. Barskiy[1,2,3]*

Zero- to ultralow-field nuclear magnetic resonance (ZULF NMR) is a rapidly developing form of spectroscopy that provides rich spectroscopic information in the absence of large magnetic fields. However, signal acquisition still requires a mechanism for generating a bulk magnetic moment for detection, and the currently used methods only apply to a limited pool of chemicals or come at prohibitively high cost. We demonstrate that the parahydrogen-based SABRE (signal amplification by reversible exchange)–Relay method can be used as a more general means of generating hyperpolarized analytes for ZULF NMR by observing zero-field *J*-spectra of [^{13}C]-methanol, [1-^{13}C]-ethanol, and [2-^{13}C]-ethanol in both ^{13}C-isotopically enriched and natural abundance samples. We explore the magnetic field dependence of the SABRE-Relay efficiency and show the existence of a second maximum at 19.0 ± 0.3 mT. Despite presence of water, SABRE-Relay is used to hyperpolarize ethanol extracted from a store-bought sample of vodka (%P_H ~ 0.1%).

INTRODUCTION

Nuclear magnetic resonance (NMR) is an analytical tool with demonstrated utility across a broad range of disciplines, from analytical chemistry (*1*), to medicine (*2*–*4*), to fundamental physics (*5*–*7*). Zero- to ultralow-field (ZULF) NMR is an emerging NMR modality that can produce rich spectroscopic information without the need for large magnetic fields (*8*, *9*). This comes with some advantages over high-field NMR, such as the ability to detect NMR signals in the presence of conductive materials (e.g., metals) and in heterogeneous environments without losing spectral resolution (*10*). ZULF NMR uses noninductive sensors, typically optically pumped magnetometers (OPMs) (*11*), which are highly sensitive (10 to 20 fT/Hz$^{1/2}$) (*12*), easy to handle (*13*), and commercially available (*14*); this recent development now makes it straightforward to assemble stand-alone ZULF NMR spectrometers (*15*).

NMR spectra of molecules at zero field, known as *J*-spectra, arise from heteronuclear *J*-couplings between spin-active nuclei (*16*, *17*). Solution-state *J*-spectra of molecules containing spin-½ heteronuclei appear as groups of peaks with narrow linewidth (0.01 to 0.5 Hz), at frequencies that are dependent on the topology of the scalar couplings (*J*-couplings) between the spins. Using the Pople notation (*18*), an XA_2 group such as a $^{13}CH_2$ (methylene) group displays one peak at $1.5J_{CH}$ in a *J*-spectrum, while an XA_3 group such as a $^{13}CH_3$ (methyl) group displays two peaks: one at the heteronuclear coupling frequency, J_{CH}, and the other at twice this value, $2J_{CH}$ (*8*). Spectra of more complex molecules containing different types of interacting groups are complicated further by additional splittings because of multiple bond *J*-couplings between neighboring spins. Despite their apparent complexity, *J*-spectra offer unique information, allowing chemical identification based on the topology of field-independent scalar coupling between spins that makes them akin to "molecular fingerprints" (*19*).

A promising aspect of ZULF NMR is the potential to minimize the size and cost of NMR spectrometers compared to high-field (including benchtop) counterparts, paving the way for their use beyond chemical laboratories (*15*). As of 2022, ZULF NMR spectrometers can be built for about half the cost (or slightly less) of a typical benchtop NMR spectrometer. However, a considerable challenge is still present in the current iteration of ZULF NMR spectrometers that poses a constraint on their minimum achievable weight and overall size: The system under study must be externally polarized before the signal can be detected. The approach of allowing a sample to reach thermal equilibrium polarization in a large external magnetic field before zero-field detection yields low polarization ($P_{1H} \sim 10^{-5}$ at 2 T) and is detrimental to portability, so alternative avenues for generating substantial NMR signals are required.

Hyperpolarization presents an alternative to the brute-force approach, and techniques such as PHIP (parahydrogen-induced polarization) (*20*), SABRE (signal amplification by reversible exchange) (*21*–*23*), and *d*DNP (dissolution dynamic nuclear polarization) (*24*) have already been shown to produce sufficient signal for detection in the ZULF regime (*25*–*28*). SABRE is especially well suited for this because (i) it is based on chemical interactions of parahydrogen (pH_2), which can be quickly and inexpensively produced (*22*), (ii) hyperpolarization can be generated multiple times in the same sample allowing for signal averaging from many experiments, and (iii) transfer of polarization from pH_2 to heteronuclei such as ^{15}N and ^{13}C typically occurs at fields in the microtesla (μT) regime (0.1 to 1.0 μT for ^{15}N and ^{13}C), which is synergistically compatible with ZULF NMR detection requirements such as shielding from Earth's magnetic field (*29*, *30*).

Central to the SABRE technique is an Ir metal complex, referred to as the polarization transfer catalyst, that mediates the transfer of nuclear spin order from pH_2 to a transiently bound substrate. The scope of substrates that can be hyperpolarized by SABRE is limited by the requirement that the substrate must reversibly bind and dissociate from the complex on a suitable time scale, ranging from milliseconds to seconds (*31*). However, the recent introduction of SABRE-Relay has ameliorated this limitation: Polarization is transferred

[1]Institut für Physik, Johannes Gutenberg Universität Mainz, 55128 Mainz, Germany. [2]Helmholtz Institut Mainz, 55128 Mainz, Germany. [3]GSI Helmholtzzentrum für Schwerionenforschung, Darmstadt, Germany. [4]Institute for Bioengineering of Catalonia, Barcelona Institute of Science and Technology, 08028 Barcelona, Spain. [5]École normale supérieure, Paris Sciences et Lettres University, 75005 Paris, France. [6]University of California at Berkeley, Berkeley, CA 94720-7300, USA.
*Corresponding author. Email: dbarskiy@uni-mainz.de

from a carrier molecule (which can be directly polarized by SABRE) to a secondary substrate through binding of a second metal complex or through proton exchange (*32*, *33*). In this work, we only consider the latter method (Fig. 1A). This innovation, along with the even more recent PHIP-X technique (*34*), has expanded the pool of polarizable substrates to encompass a wide class of molecules with exchangeable protons. Here, we demonstrate that chemical exchange effects (*27*, *35*) do not inhibit ZULF NMR detection of hyperpolarized, primary alcohols in organic solvent dichloromethane (DCM), where the polarization is derived from exchangeable protons of the hydroxyl group.

RESULTS

In this work, two NMR detection principles were used: inductive detection at 1 or 1.4 T using benchtop NMR spectrometers and detection using a commercially available OPM in ZULF conditions

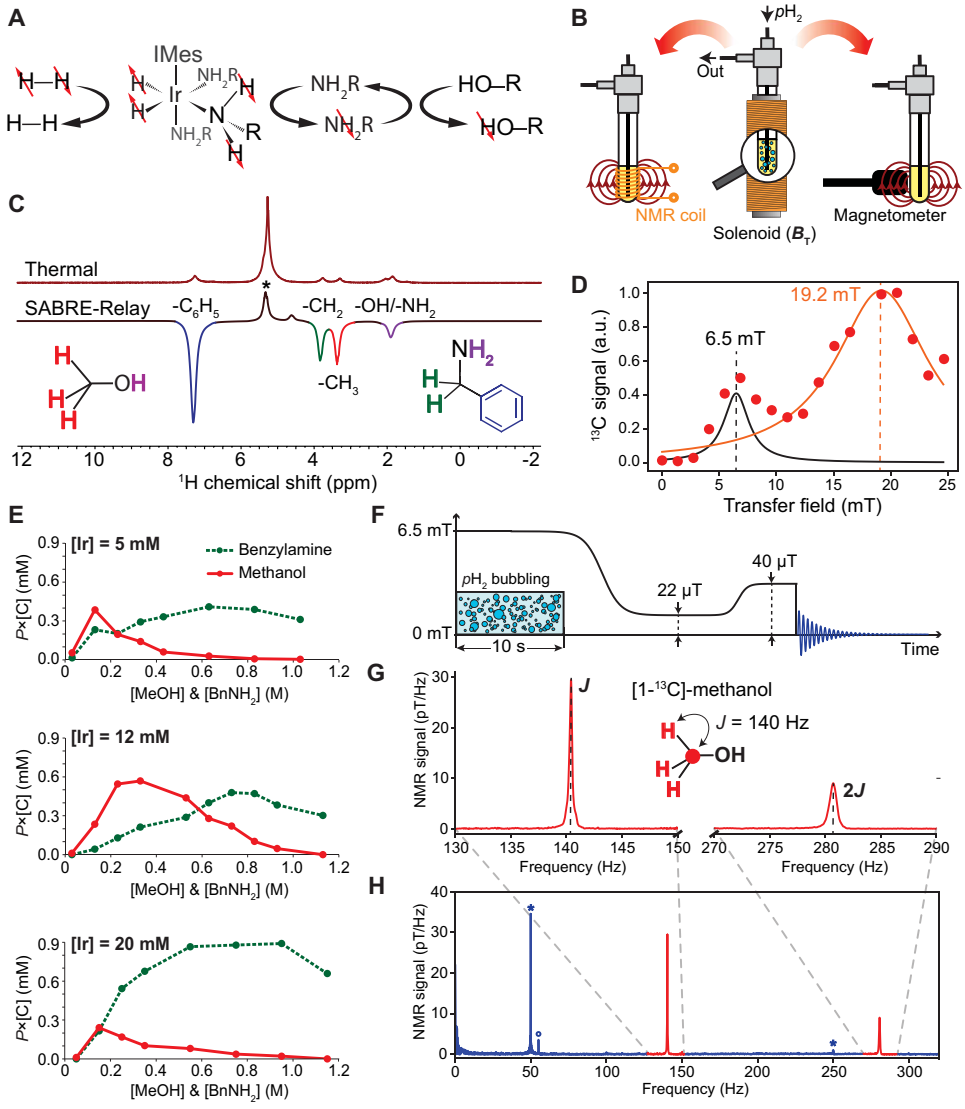

Fig. 1. SABRE-Relay optimization and ZULF NMR measurements of methanol. (**A**) Molecular diagram of the SABRE-Relay process: Parahydrogen (pH_2) coordinates with the Ir catalyst to form [Ir(IMes)($BnNH_2$)$_3$$H_2$] (denoted [Ir] below), allowing the transfer of spin order onto the bound substrate, benzylamine ($BnNH_2$), and to a second substrate via proton exchange. (**B**) Schematic of the experiment showing two possible detection modes: (left) inductive detection used in this work using a benchtop NMR spectrometer (40 or 60 MHz); (right) detection of NMR with an OPM in the ZULF regime. (**C**) ^{1}H NMR spectrum (1.4 T) of methanol and benzylamine (both 230 mM) in DCM (top) at thermal equilibrium polarization and (bottom) a SABRE-Relay hyperpolarized (B_T ~ 7 mT, 10-s bubbling, 60 SCCM pH_2 at 5 bar) spectrum of the same sample. (**D**) Magnetic field dependence of SABRE-Relay–derived hyperpolarization of methanol detected via ^{13}C DEPT at 1.4 T showing two clear maxima. a.u., arbitrary units. (**E**) Methanol molar polarization as a function of methanol and benzylamine concentrations. Both chemicals were increased in tandem by adding concentrated stock solution to the activated [Ir] catalyst. (**F**) ZULF NMR event sequence: bubbling of pH_2 into the sample at 6.5 mT for 10 s followed by a drop in field induced by sample insertion into magnetic shield through the solenoid (22 μT) before reaching the 40-μT Helmholtz coil field. This was nonadiabatically switched off immediately before acquisition of the NMR signal. (**G**) ZULF NMR spectrum (64 scans) of SABRE-Relay–polarized methanol-^{13}C (230 mM methanol, 230 mM benzylamine, 12 mM [Ir]) showing peaks at J and 2J, where J is the heteronuclear $^1J_{CH}$ coupling. (**H**) Full ZULF NMR spectrum (64 scans) showing 50-Hz noise peak and overtones from transmission-line noise (*) and noise arising from the laser of the OPM sensor and the temperature-stabilization circuit (°).

(Fig. 1B). Benchtop NMR experiments were performed to optimize the chemical composition of the system and experimental parameters (e.g., pH_2 pressure and flow rate, polarization transfer field) for obtaining maximal molar polarization, defined as the product of polarization and the concentration of the nuclei contributing to the signal (*36*) (see discussion). ZULF NMR spectra were recorded on the sample with optimal chemical composition.

Detection of SABRE-Relay NMR signals from methanol at 1 T

Figure 1C illustrates the enhancement of methanol NMR signals via SABRE-Relay on a sample of 230 mM methanol, 230 mM benzylamine, and 12 mM SABRE catalyst (see Materials and Methods) in DCM. pH_2 was bubbled through the sample at 4 bar for 10 s in a 7-mT field (B_T), followed by transfer to a 1-T benchtop NMR magnet for the acquisition of the hyperpolarization enhanced signal. After the signals had fully relaxed, a spectrum was acquired of the sample at thermal equilibrium polarization. Note that the hyperpolarization-enhanced ^{1}H NMR signals of the carrier amine benzylamine ($BnNH_2$) and methanol are negative. Because of intermolecular proton exchange between -OH and -NH_2 groups in DCM, their NMR resonances coalesce into a single broad line.

Field dependence of SABRE-Relay hyperpolarization

To optimize for NMR signal enhancement, SABRE-Relay experiments were performed at various polarization transfer fields (B_T). After a 10-s period of pH_2 bubbling at B_T, a sample—containing benzylamine, methanol, and polarization transfer catalyst [Ir(IMes)(COD)Cl] (denoted as [Ir]), all at natural isotopic abundance—was transferred to a 1.4-T NMR magnet, and the ^{13}C signal was detected after application of a DEPT (distortionless enhancement by polarization transfer) pulse sequence (*37*). Choosing an interpulse delay of 1/(2*J*) in DEPT allowed transferring polarization from ^{1}H to ^{13}C spins in -CH_3 groups of methanol. Plotting the ^{13}C peak integrals as a function of transfer field and fitting the data with the sum of two Lorentzians revealed two distinct maxima at 6.5 ± 0.3 and 19.2 ± 0.3 mT (Fig. 1D). ^{13}C NMR signal was used for spectral clarity, because of overlap of benzylamine and methanol resonances in the ^{1}H spectrum.

Optimization of methanol and ethanol ^{1}H molar polarization

Hyperpolarization derived from SABRE-Relay has been shown to be highly dependent on the concentrations of substrate, carrier amine, and catalyst, and we verified with experiments (fig. S7) that a mixture with methanol concentration in slight excess relative to benzylamine concentration (1:1 to 2:1 methanol:benzylamine) gives the highest methanol polarization. To further increase the observable signal by optimizing methanol molar polarization, the concentrations of methanol and benzylamine were varied (Fig. 1E). We observed that increasing the concentrations of both methanol and benzylamine ($BnNH_2$) yielded maximal $BnNH_2$ molar polarization at 0.6 to 0.8 M $BnNH_2$ concentration; higher SABRE catalyst concentration gave larger $BnNH_2$ ^{1}H NMR signals. This was not the case for the molar polarization (i.e., polarization × concentration) of methanol, which was larger at a catalyst concentration of 12 mM, resulting in molar polarization of 0.2 at 300 mM (Fig. 1E).

Similarly, to optimize ^{1}H molar polarization of ethanol using a 1-T benchtop NMR spectrometer, we gradually increased the ethanol concentration by pipetting small amounts of ethanol into an activated SABRE-Relay solution (12 mM Ir catalyst, 230 mM benzylamine, and 130 mM ethanol) at a transfer field of 6.5 mT. It was found that a ratio of ~2:1 ethanol:benzylamine provided the largest polarization (0.1%) and molar polarization (0.6 mM).

ZULF NMR detection of SABRE-Relay–polarized [^{13}C]-methanol

ZULF NMR detection of SABRE-Relay–polarized, isotopically enriched (99% ^{13}C), and nonlabeled (1.1% ^{13}C) methanol was performed as follows: pH_2 was bubbled at 5 bar for 10 s through a solution in a solenoid (B_T = 6.5 mT) located above the μ-metal shielding of the ZULF NMR spectrometer. After the pH_2 flow was ceased, the sample was automatically transferred through a guiding solenoid (22 μT) to the zero-field region in which a magnetic field of 40 μT was being applied in the direction of the sensitive axis of the magnetometer. This magnetic field was then nonadiabatically switched off (in 10 μs) to generate an observable signal decay that was picked up by the magnetometer (Fig. 1F). Via automation, the sequence could be repeated to accumulate multiple signal acquisition scans. Fourier transform of the free decay gives ZULF NMR spectra in which characteristic resonances of [^{13}C]-methanol are observed at 140.084 ± 0.001 and 280.156 ± 0.002 Hz in 64 scans, obtained in ~22 min of measurement for an isotopically enriched sample (Fig. 1G). A *J*-spectrum of [^{13}C]-methanol at natural ^{13}C abundance (~1.1%) is presented in fig. S14A, where 400 scans (~2.2 hours total measurement time) were averaged using a similar experimental scheme as mentioned above.

ZULF NMR detection of SABRE-Relay NMR signals from [^{13}C]-ethanol

The polarization methodology developed for the observation of ZULF NMR signals from [^{13}C]-methanol was applied to [^{13}C]-ethanol. When [1-^{13}C]-ethanol was used as a SABRE-Relay substrate, two groups of peaks are observed in *J*-spectra (Fig. 2A). The first group of peaks are low-frequency peaks within the 3- to 11-Hz region, which arise from the relatively small $2J_{CH}$ coupling. The second group of peaks are high-frequency peaks with major resonances lying between 200 and 230 Hz, which corresponds to an expected transition at (3/2) J_{13C1H} = 211.278 Hz (J_{13C1H} = 140.852 ± 0.001 Hz) (*38*), split by the proton-proton *J*-couplings. Experimentally observed spectra are compared with the results of numerical spin dynamical simulations (see the Supplementary Materials for details). When [2-^{13}C]-ethanol was used as a SABRE-Relay substrate, three groups of peaks can be distinguished (Fig. 2B). The first group of peaks are low-frequency peaks less than 20 Hz. The second group of peaks are centered on J_{13C1H} = 125.257 ± 0.001 Hz (*38*) from the CH_3 group of ethanol. The third group of peaks lie between 230 and 260 Hz, corresponding to an expected transition around at $2J_{13C1H}$. Experimentally observed spectra are compared with the results of numerical calculations of spin dynamics (MATLAB code available in the Supplementary Materials) starting with equal polarization of all protons in the molecule. We note that various initial polarization states were used for simulations, and the results are presented in the Supplementary Materials and discussed further in the text.

ZULF NMR relaxometry of hyperpolarization-enhanced NMR signals from [^{13}C]-ethanol

Relaxation of hyperpolarization-enhanced ZULF NMR signals of [1-^{13}C]-ethanol and [2-^{13}C]-ethanol (Fig. 2C) was monitored by

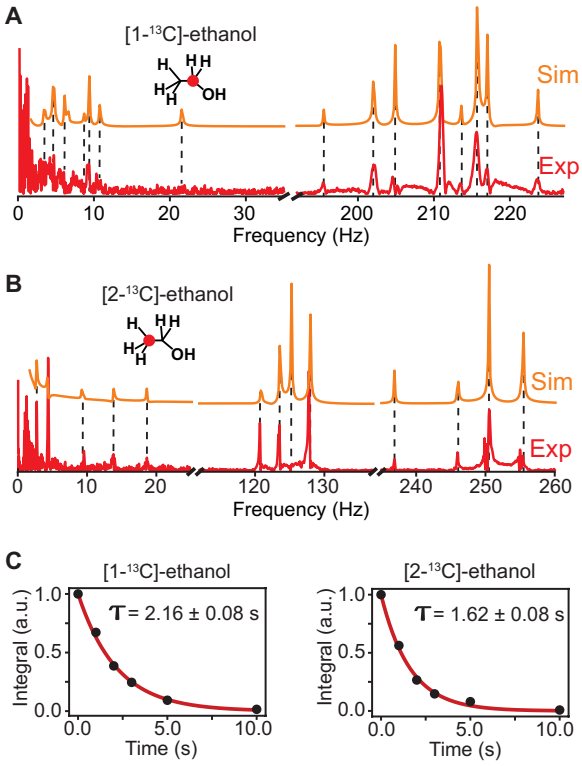

Fig. 2. SABRE-Relay of ^{13}C-labeled ethanol with detection in the ZULF regime. (**A** and **B**) Simulated and experimental zero-field *J*-spectra (64 scans) of [1-^{13}C]-ethanol and [2-^{13}C]-ethanol (230 mM) hyperpolarized by SABRE-Relay separately using the carrier amine benzylamine. Red dots represent the positions of the [^{13}C] nucleus. (**C**) Relaxometry of [1-^{13}C]- and [2-^{13}C]-ethanol at zero field obtained by integrating peaks at 210 and 128 Hz, respectively, and then fitting the results with a monoexponential decay function with the stated time constant. Each data point represents the sum of four scans.

incrementing a time delay between the sample arrival to the ZULF region and the beginning of spectral acquisition. Integrating the largest spectral peaks (at 210 and 250 Hz for [1-^{13}C]-ethanol and [2-^{13}C]-ethanol, respectively) and fitting the corresponding time traces with monoexponential decay functions gave relaxation time constants of 2.16 ± 0.08 and 1.62 ± 0.08 s, respectively. These short relaxation times are expected because the ^{1}H and ^{13}C spins are close in space, leading to efficient intramolecular dipole-dipole relaxation.

SABRE-Relay hyperpolarization of ethanol extracted from vodka

Ethanol was extracted from store-bought vodka (Puschkin; 37.5% ethanol v/v) by mixing equal volumes of vodka with DCM. The ethanol concentration in the resulting organic layer was determined by comparing integrals of the solvent peak (DCM) and the methyl group of ethanol. This solution was then mixed with activated SABRE solution to a final concentration of 260 mM benzylamine, 650 mM ethanol, and 12 mM [Ir(IMes)(COD)]Cl in DCM (*39*). A SABRE-Relay–enhanced ^{1}H NMR spectrum (1 T) recorded for the same sample after 10 s of pH_2 bubbling at 6.5 mT shows substantially enhanced ^{1}H resonances of all protons in $BnNH_2$ and in ethanol (fig. S13). A similar procedure was used to generate samples for detection of non–^{13}C-enriched ethanol with ZULF NMR, where each acquisition took approximately 20 s for shuttling, detection, and pH_2 bubbling. Figure S14B shows the *J*-spectrum of a sample containing ethanol (600 mM) from vodka with benzylamine (260 mM) and Ir catalyst (12 mM) after 400 transients (~2.2 hours total experimental time). Figure 3C and fig. S14C both show the *J*-spectrum of a mixture of ethanol (750 mM) from vodka and methanol (750 mM) at natural isotopic abundance with benzylamine (250 mM) and Ir (12 mM) in DCM after 1500 transients recorded over ~8.3 hours. Because of the limited solubility, concentration of water in DCM in these experiments did not exceed 200 mM (measured by ^{1}H NMR).

DISCUSSION

Inductive and noninductive detection of SABRE-Relay–enhanced NMR signals

The two detection modalities (inductive and noninductive) demonstrated in Fig. 1B are compatible with each other such that the same sample can be used with either modality. A modular system for pH_2 sparging and sample shuttling may be switched between the two modalities on demand within minutes. Using a benchtop NMR system for optimizing SABRE-Relay is advantageous for many reasons, including rapid spectral acquisition, excellent accessibility, and reproducibility, which allows the rapid alteration of parameters to maximize ^{1}H NMR polarization. This greatly helps to optimize system parameters such as temperature, concentrations, pH_2 pressure, and flow rate before attempting ZULF NMR measurements.

We choose molar polarization as a figure of merit for optimization experiments (Fig. 1E). Molar polarization is a product of nuclear spin polarization (units of polarization, dimensionless) and concentration (mol/liter). Polarization itself is a good figure of merit for many experiments in which the hyperpolarized target is produced in similar concentration in each experiment (e.g., as is often the case with dissolution DNP) or in which the concentration is limited by a biological process or chemical reaction. However, molar polarization is better suited for cases in which the largest signal from a fixed-volume sample is desired.

The magnetic field profile used for implementing OPM-based NMR detection is shown in Fig. 1F. Parahydrogen was bubbled through a SABRE mixture at 6.5 or 19.2 mT (for polarization buildup), and then a sample was mechanically transferred to the zero-field region. Inside an enclosure made of four layers of μ-metal shielding, a solenoid coil provided a 22-μT field between the shield layers for sample transfer, and an additional Helmholtz coil was placed to provide a field of 40 μT oriented in the direction of the OPM-sensitive axis (located perpendicular to the long axis of the NMR tube) to be the dominant field at the sample location before detection. This field was then nonadiabatically switched off within 10 μs, and the signal was measured with the QuSpin Zero-Field Magnetometer OPM. In principle, an alternative detection approach can be successfully used where short pulses of magnetic field can generate initial coherence for signal detection. We carried out experiments using this pulsed approach, and the data are presented in fig. S11. One should note that while OPMs are used in this work as an example of noninductive sensors, other sensors such as superconducting quantum interference device, magneto-resistive sensors, or NV centers in diamonds can be used; examples of ZULF NMR with such sensors have been demonstrated in the literature (*40*–*42*).

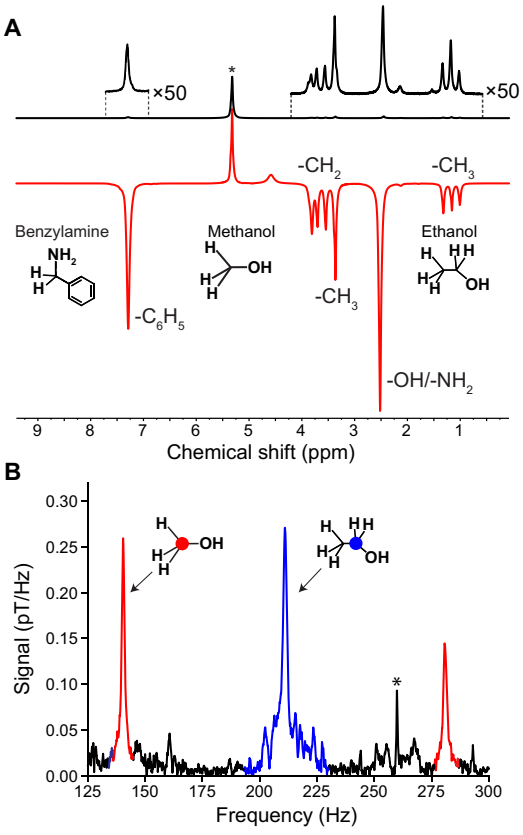

Fig. 3. Hyperpolarization and detection of a methanol/ethanol mixture at natural isotopic abundance. (**A**) High-field (1 T) ^{1}H NMR spectra of a thermally polarized (top) and SABRE-Relay–polarized (bottom) sample containing ethanol (750 mM) extracted from vodka and methanol (750 mM) at natural isotopic abundance with benzylamine (250 mM) and Ir catalyst (12 mM). The SABRE spectrum was observed after 10 s of bubbling with parahydrogen in a field of 19 mT at 5 bar and 60 SCCM. (**B**) ZULF NMR spectrum of the same sample following 1500 scans and similar SABRE parameters as in (A). The peaks of methanol at 140 and 280 Hz represent J_{CH} and $2J_{CH}$, and the cluster of peaks surrounding 210 Hz arise from the AX_2 spin system of [1-^{13}C]-ethanol ($3/2{*}J_{CH}$, $J = 140$ Hz). Peaks for [2-^{13}C]-ethanol are visible around 255 Hz, although markedly less clear than those of the other ethanol isotopomer; (*) denotes peak from an unknown source.

Mechanism of SABRE-Relay polarization transfer via benzylamine

The mechanism of polarization transfer to protons in conventional SABRE is generally well understood. When the *J*-coupling value between hydride nuclei ($J_{HH} \cong -7$ Hz) in the SABRE complex matches the Larmor frequency difference between the hydride and bound substrate spins, the singlet spin order of pH_2 can be converted into observable magnetization of the substrate (*43*). The sign of magnetization depends on the relative sign of the *J*-coupling and the frequency difference. Because these chemical shift differences are similar for a variety of substrates (because of the large separation of ~30 parts per million units) and J_{HH} is generally independent of the nature of the bound substrate, the value of the magnetic field, on the order of 6 to 7 mT, optimal for polarization transfer is virtually the same for all SABRE substrates (*44*). In SABRE-Relay, the polarization of the protons in an NH_2 group of benzylamine is transferred to the methanol because of chemical exchange. This explains the spectrum shown in Fig. 1C, where resonances of -NH_2, -CH_2, and benzyl groups of $BnNH_2$ as well as -CH_3 and -OH groups of methanol all demonstrate enhanced emissive signals. The increasing trend in the SABRE-Relay enhancement of primary alcohols was demonstrated previously at fields of 12 to 14 mT (*45*). The investigated region up to 25 mT reported here reveals the presence of two maxima arising from the SABRE process via benzylamine (Fig. 1D).

The first peak at 6.5 mT is the expected maximum corresponding to the symmetric active SABRE complex [Ir(IMes)($BnNH_2$)$_3H_2$] (Fig. 1A) and the conventional polarization transfer mechanism as described above (*46*). The nature of the second peak is still under investigation but may have two possible explanations. First, this maximum may originate from an asymmetric Ir complex operating under a mechanism similar to the one described by Emondts *et al.* (*47*). This mechanism, called NEPTUN (nuclear exchange polarization by transposing unattached nuclei), is based on direct hydride transfer from the catalyst to an axially bound substrate that has a labile proton (fig. S12) (*47*). This requires formation of an asymmetric complex where the chemical equivalence of the bound hydrides is broken, forming an AB spin system, which then evolves magnetization that can be detected in the substrate following hydride transfer. The second explanation involves a magnetic field dependence that is complicated by the presence of a heteronucleus, such as ^{15}N. A heteronucleus present in the active SABRE complex can split a single maximum in the magnetic field dependence into two (*30*, *48*). Maximum efficiency of the NEPTUN effect is predicted when the chemical shift difference between the hydrides in an asymmetric complex is equal to the *J*-coupling between them. Alternatively, the splitting of the field maxima for an AA′BX system would depend on the value of $|J_{AX} - J_{A'X}|$. Our attempts to directly observe the hydride resonances indicative of the NEPTUN effect have not been successful, and the investigation as to whether natural abundance of ^{15}N nuclei in benzylamine (~0.36% of naturally occurring nitrogen) is enough to cause the observed effect is still ongoing.

It was reported that the presence of water detrimentally affects SABRE-Relay efficiency (*33*). This is possibly due to the accelerated proton exchange, which may affect protons in the carrier amine during the time it is bound to the complex, thus altering the spin dynamics (*46*). Our findings in the conditions studied show that ^{1}H NMR signal enhancement of methanol is decreased by a factor of ~2 after addition of 5 μl of water to 0.5 ml of the SABRE-Relay sample with $B_T \sim 6$ mT (fig. S4). When the second maximum at 19.2 mT in the SABRE-Relay field profile was used for polarization buildup, the presence of water did not significantly alter the intensity of methanol hyperpolarization. However, studies with ethanol as a substrate revealed an insignificant effect of the polarization transfer field upon addition of three subsequent 5-μl aliquots of water (fig. S4). The dependence on H_2O concentration may indirectly support the hypothesis involving proton exchange since it is the spins from water that are predominantly expected to be polarized by the NEPTUN effect. However, we note that magnetic field dependence of the SABRE process of $BnNH_2$ alone (no methanol added) also revealed the presence of the two distinct maxima (fig. S5). This observation casts doubts that polarization of alcohols in the conditions tested in this paper is due to direct binding to the complex; naturally abundant ^{15}N nuclei are likely causing the observed phenomenon; however, investigation of this effect is beyond the scope of this paper.

Zero-field NMR spectroscopy of SABRE-Relay–polarized alcohols

Experimentally observable ZULF NMR spectra of [^{13}C]-methanol and [^{13}C]-ethanol match well with the theoretically calculated spectra (Fig. 2, A and B). On top of the main one-bond heteronuclear *J*-coupling, the presence of additional *J*-couplings between spins from different chemical groups in ethanol generates a complex spectral pattern that is generally well reproduced. However, one can see that not all features in *J*-spectra are reproduced by the simulated spectra.

While, in general, the positions of the peaks in experimental *J*-spectra match well to the calculated ones and the ones demonstrated previously (*38*), the intensity of the lines deviates significantly from calculations. These deviations in peak amplitude are seen for both [1-^{13}C]-ethanol and [2-^{13}C]-ethanol ZULF NMR spectra; they are especially well pronounced for the latter in the middle frequency region (for example, note the absence of the peak at 125 Hz in Fig. 2B). This transition is well characterized and corresponds to the flip of carbon-13 spins while the protons in the -CH_2- group remain in the state with total spin 0 (*38*). This indicates that the singlet state of the spins in the CH_2 group is not overpopulated during the SABRE-Relay process, and proton magnetization is a likely starting condition before evolution in the ZULF region.

We further investigated this by simulating a variety of ZULF NMR spectra for [1-^{13}C]-ethanol and [2-^{13}C]-ethanol starting with different initial proton spin orders (figs. S2 and S3). Polarization of all protons as a starting condition was compared to the polarization of protons in CH_3 and CH_2 groups separately. While polarization of all ^{1}H spin generally fits the experimental observations, one can see that, for example, a spectral pattern observed for [2-^{13}C]-ethanol is reproduced better when polarization of CH_2 group alone (and not CH_3 group) is considered. This observation highlights that protons cannot always be considered strongly coupled at low fields when heteronuclei such as ^{13}C are involved in the process. It has been shown recently that heteronuclear spin-spin interactions suppress the strong coupling regime even when the external field is relatively low because ^{13}C spins modify the energy level structure (*49*). This means that the SABRE-Relay process via proton exchange, when applied to [2-^{13}C]-ethanol at 6.5 mT, would only polarize proton spins in the CH_2 group, leaving protons in the $^{13}CH_3$ group unpolarized (or polarized to a significantly lower degree). The actual experiments involved sample transfer through the near-zero-field regime before the measurement (Fig. 1F); thus, partial redistribution of polarization between all the spins is expected. This may explain the discrepancy between the experimentally observed spectra and simulations. However, future studies are necessary to understand the exact nature of polarization transfer during the SABRE-Relay process with ZULF NMR measurement, to obtain the largest signal for the substrate of interest, and to prepare spin states with extended lifetimes (such as those found in -$^{13}CH_2$- and -$^{13}CH_3$ groups).

Hyperpolarization and affordable NMR detection of alcohols from extracted samples

The ^{1}H polarization levels of 0.1% demonstrated here for ethanol obtained from the store-bought vodka sample (Fig. 3 and fig. S13) highlight the analytical potential of the SABRE-Relay technique for enhancing signals of substances extracted from commercial materials. The advantage of SABRE compared to other hyperpolarization techniques such as PHIP and *d*DNP lies in the fact that the same sample can be polarized multiple times by bubbling a fresh portion of pH_2 gas through the solution and the signal can be averaged out, increasing the signal-to-noise ratio. One may note that the intensity of the ^{1}H NMR peak from the solvent is enhanced as is evident from a single-scan SABRE-Relay spectrum compared to the spectrum recorded at thermal equilibrium (fig. S13). We assign this effect to the intermolecular spin polarization–induced nuclear Overhauser effect between hyperpolarized analytes and DCM molecules, which is typical for highly hyperpolarized (e.g., magnetized) samples (*50*).

Overall, we demonstrate that improving effectiveness of hyperpolarization in the SABRE-Relay methodology enables efficient ZULF NMR measurements of molecules having exchangeable protons. Hyperpolarization of [1-^{13}C]-methanol, [1-^{13}C]-ethanol, and [2-^{13}C]-ethanol and subsequent ZULF NMR detection of the *J*-spectra of these molecules were demonstrated and confirmed by numerical simulations. A new maximum in the SABRE field dependence was found, which may be due to the presence of ^{15}N nuclei at the natural isotopic abundance in benzylamine. These results demonstrate analytical capabilities of ZULF NMR using SABRE-Relay–based hyperpolarization for applications beyond research laboratories. Further improvements are possible by adiabatic and nonadiabatic field manipulations and by optimal control approaches to effectively simplify *J*-spectra.

MATERIALS AND METHODS

Optimization

Solutions of methanol, benzylamine, and [Ir(COD)(IMes)Cl] ([Ir]) catalyst were prepared in DCM (Sigma-Aldrich) and hydrogenated at parahydrogen (pH_2) pressures from 1 to 6 bar. Hydrogenation was carried out by bubbling the solution with pH_2 via a 0.9-mm OD (outer diameter) PTFE (polytetrafluoroethylene) capillary inserted into a pressurizable 5-mm OD NMR tube fitted with a modified Young's valve cap. Flow of pH_2 was controlled by a mass flow controller (Sierra Instruments SmartTrak 100) generally set between 20 SCCM (standard cubic centimeter per minute) for activation of the polarization transfer catalyst, [Ir] and up to 90 SCCM for SABRE-Relay experiments, while pressure in the system was controlled via back pressure regulator (Swagelok). Spectra were recorded in a 1.4-T SpinSolve benchtop spectrometer (Magritek) for optimization of reaction parameters. The timing of bubbling was controlled electronically via an Arduino Uno, which was also used to initiate NMR spectral acquisition. The adjustable SABRE transfer field was provided by a hand-wound solenoid (up to ~22 mT) and a custom-built variable Halbach array of transversely oriented magnets capable of generating a field from 1 to 101 mT.

For concentration-based optimization studies, a stock solution was added stepwise to increase the concentrations of benzylamine and methanol. We began by adjusting the concentration of benzylamine while maintaining a methanol concentration of 30 mM by adding 10 μl of a concentrated benzylamine stock directly to the sample to increase benzylamine concentration in steps of 20 mM from 10 to 110 mM (sample volume, 500 μl). We repeated the same procedure for methanol while holding the benzylamine concentration at 30 mM and found that a 1:1 ratio provided the optimum methanol molar polarization, which we define as the substrate concentration times its polarization, supporting optimization work done by Rayner *et al.* (*45*). Samples were shuttled either by hand or by a robotic arm fitted with a three-dimensional printed adapter to hold the pH_2 bubbling apparatus.

ZULF NMR

Measurements were made using a commercially available OPM (QuSpin) inserted into a Helmholtz array with two orthogonal coils used to generate pulses. External magnetic fields were blocked by an MS-1 μ-metal shield from Twinleaf, and shimming of any interior residual field was conducted using built-in shimming coils. Polarization was generated by bubbling with >99% parahydrogen at 5 bar for 10 s, 60 SCCM in a 6- to 20-mT field generated by an axially oriented solenoid placed above the shield. The sample was shuttled into the sensor region using an automated robotic setup (results will be published elsewhere); variable static field was applied to control the efficiency of spin order transfer in the SABRE-Relay process. Each acquisition-shuttling cycle had a duration of approximately 20 s. All ZULF NMR spectra presented in the paper are shown in the magnitude mode.

Collection of *J*-spectra of nonisotopically labeled methanol and ethanol samples was aided by the addition of a presaturating chamber containing a small volume of solvent with substrate through which the parahydrogen was directed before bubbling through the sample chamber. This is necessary because both the solvent (DCM) and substrate (methanol and, to a lesser extent, ethanol) evaporate quickly during pH_2 bubbling without presaturation (*26*). The addition of the presaturator more than doubled the possible acquisition time, allowing hundreds of acquisitions to be taken per sample before significant loss of signal.

SUPPLEMENTARY MATERIALS

Supplementary material for this article is available at https://science.org/doi/10.1126/sciadv.abp9242

REFERENCES AND NOTES

1. P. Giraudeau, Challenges and perspectives in quantitative NMR. *Magn. Reson. Chem.* **55**, 61–69 (2017).
2. E. Cavallari, C. Carrera, S. Aime, F. Reineri, Metabolic studies of tumor cells using [1-^{13}C] pyruvate hyperpolarized by means of PHIP-side arm hydrogenation. *ChemPhysChem* **20**, 318–325 (2019).
3. P. J. Basser, D. K. Jones, Diffusion-tensor MRI: Theory, experimental design and data analysis—A technical review. *NMR Biomed.* **15**, 456–467 (2002).
4. R. Damadian, M. Goldsmith, L. Minkoff, NMR in cancer: XVI. FONAR image of the live human body. *Physiol. Chem. Phys.* **9**, 97–100 (1977).
5. J. Eills, J. W. Blanchard, L. Bougas, M. G. Kozlov, A. Pines, D. Budker, Measuring molecular parity nonconservation using nuclear-magnetic-resonance spectroscopy. *Phys. Rev. A.* **96**, 042119 (2017).
6. A. L. Barra, J. B. Robert, Parity non-conservation and NMR parameters. *Mol. Phys.* **88**, 875–886 (1996).
7. V. Weijo, P. Manninen, J. Vaara, Perturbational calculations of parity-violating effects in nuclear-magnetic-resonance parameters. *J. Chem. Phys.* **123**, 054501 (2005).
8. J. W. Blanchard, D. Budker, A. Trabesinger, Lower than low: Perspectives on zero- to ultralow-field nuclear magnetic resonance. *J. Magn. Reson.* **323**, 106886 (2021).
9. J. W. Blanchard, D. Budker, Zero- to utltralow-field NMR. *eMagRes.* **5**, 1395–1410 (2016).
10. D. B. Burueva, J. Eills, J. W. Blanchard, A. Garcon, R. Picazo-Frutos, K. V. Kovtunov, I. V. Koptyug, D. Budker, Chemical reaction monitoring using zero-field nuclear magnetic resonance enables study of heterogeneous samples in metal containers. *Angew. Chemie Int. Ed.* **59**, 17026–17032 (2020).
11. D. Budker, M. Romalis, Optical magnetometry. *Nat. Phys.* **3**, 227–234 (2007).
12. M. C. D. Tayler, T. Theis, T. F. Sjolander, J. W. Blanchard, A. Kentner, S. Pustelny, A. Pines, D. Budker, Invited Review Article: Instrumentation for nuclear magnetic resonance in zero and ultralow magnetic field. *Rev. Sci. Instrum.* **88**, 091101 (2017).
13. E. Boto, N. Holmes, J. Leggett, G. Roberts, V. Shah, S. S. Meyer, L. D. Muñoz, K. J. Mullinger, T. M. Tierney, S. Bestmann, G. R. Barnes, R. Bowtell, M. J. Brookes, Moving magnetoencephalography towards real-world applications with a wearable system. *Nature* **555**, 657–661 (2018).
14. J. W. Blanchard, T. Wu, J. Eills, Y. Hu, D. Budker, Zero- to ultralow-field nuclear magnetic resonance J-spectroscopy with commercial atomic magnetometers. *J. Magn. Reson.* **314**, 106723 (2020).
15. P. Put, S. Pustelny, D. Budker, E. Druga, T. F. Sjolander, A. Pines, D. A. Barskiy, Zero- to ultralow-field NMR spectroscopy of small biomolecules. *Anal. Chem.* **93**, 3226–3232 (2021).
16. M. C. Butler, M. P. Ledbetter, T. Theis, J. W. Blanchard, D. Budker, A. Pines, Multiplets at zero magnetic field: The geometry of zero-field NMR. *J. Chem. Phys.* **138**, 184202 (2013).
17. T. Theis, J. W. Blanchard, M. C. Butler, M. P. Ledbetter, D. Budker, A. Pines, Chemical analysis using *J*-coupling multiplets in zero-field NMR. *Chem. Phys. Lett.* **580**, 160–165 (2013).
18. H. J. Bernstein, J. A. Pople, W. G. Schneider, The analysis of nuclear magnetic resonance spectra: I. Systems of two and three nuclei. *Can. J. Chem.* **35**, 67–83 (1957).
19. J. W. Blanchard, M. P. Ledbetter, T. Theis, M. C. Butler, D. Budker, A. Pines, High-resolution zero-field NMR *J*-spectroscopy of aromatic compounds. *J. Am. Chem. Soc.* **135**, 3607–3612 (2013).
20. C. R. Bowers, D. P. Weitekamp, Parahydrogen and synthesis allow dramatically enhanced nuclear alignment. *J. Am. Chem. Soc.* **109**, 5541–5542 (1987).
21. K. D. Atkinson, M. J. Cowley, P. I. P. Elliott, S. B. Duckett, G. G. R. Green, J. López-Serrano, A. C. Whitwood, Spontaneous transfer of parahydrogen derived spin order to pyridine at low magnetic field. *J. Am. Chem. Soc.* **131**, 13362–13368 (2009).
22. R. W. Adams, J. A. Aguilar, K. D. Atkinson, M. J. Cowley, P. I. P. Elliott, S. B. Duckett, G. G. R. Green, I. G. Khazal, J. Lopez-Serrano, D. C. Williamson, Reversible interactions with para-hydrogen enhance NMR sensitivity by polarization transfer. *Science* **323**, 1708–1711 (2009).
23. R. W. Adams, S. B. Duckett, R. A. Green, D. C. Williamson, G. G. R. Green, A theoretical basis for spontaneous polarization transfer in non-hydrogenative parahydrogen-induced polarization. *J. Chem. Phys.* **131**, 194505 (2009).
24. J. H. Ardenkjaer-Larsen, B. Fridlund, A. Gram, G. Hansson, L. Hansson, M. H. Lerche, R. Servin, M. Thaning, K. Golman, Increase in signal-to-noise ratio of >10,000 times in liquid-state NMR. *Proc. Natl. Acad. Sci.* **100**, 10158–10163 (2003).
25. T. Theis, P. Ganssle, G. Kervern, S. Knappe, J. Kitching, M. P. Ledbetter, D. Budker, A. Pines, Parahydrogen-enhanced zero-field nuclear magnetic resonance. *Nat. Phys.* **7**, 571–575 (2011).
26. J. W. Blanchard, B. Ripka, B. A. Suslick, D. Gelevski, T. Wu, K. Münnemann, D. A. Barskiy, D. Budker, Towards large-scale steady-state enhanced nuclear magnetization with in situ detection. *Magn. Reson. Chem.* **59**, 1208–1215 (2021).
27. D. A. Barskiy, M. C. D. Tayler, I. Marco-Rius, J. Kurhanewicz, D. B. Vigneron, S. Cikrikci, A. Aydogdu, M. Reh, A. N. Pravdivtsev, J. B. Hövener, J. W. Blanchard, T. Wu, D. Budker, A. Pines, Zero-field nuclear magnetic resonance of chemically exchanging systems. *Nat. Commun.* **10**, 3002 (2019).
28. R. Picazo-Frutos, Q. Stern, J. W. Blanchard, O. Cala, M. Ceillier, S. F. Cousin, J. Eills, S. J. Elliott, S. Jannin, D. Budker, Dissolution dynamic nuclear polarization-enhanced zero-to ultralow-field nuclear magnetic resonance. *ChemRxiv* 10.26434/chemrxiv-2022-f8t03-v2 (2022).
29. T. Theis, M. L. Truong, A. M. Coffey, R. V. Shchepin, K. W. Waddell, F. Shi, B. M. Goodson, W. S. Warren, E. Y. Chekmenev, Microtesla SABRE enables 10% nitrogen-15 nuclear spin polarization. *J. Am. Chem. Soc.* **137**, 1404–1407 (2015).
30. D. A. Barskiy, S. Knecht, A. V. Yurkovskaya, K. L. Ivanov, SABRE: Chemical kinetics and spin dynamics of the formation of hyperpolarization. *Prog. Nucl. Magn. Reson. Spectrosc.* **114–115**, 33–70 (2019).
31. M. J. Cowley, R. W. Adams, K. D. Atkinson, M. C. R. Cockett, S. B. Duckett, G. G. R. Green, J. A. B. Lohman, R. Kerssebaum, D. Kilgour, R. E. Mewis, Iridium N-heterocyclic carbene complexes as efficient catalysts for magnetization transfer from para-Hydrogen. *J. Am. Chem. Soc.* **133**, 6134–6137 (2011).
32. S. S. Roy, K. M. Appleby, E. J. Fear, S. B. Duckett, SABRE-Relay: A versatile route to hyperpolarization. *J. Phys. Chem. Lett.* **9**, 1112–1117 (2018).
33. W. Iali, P. J. Rayner, S. B. Duckett, Using parahydrogen to hyperpolarize amines, amides, carboxylic acids, alcohols, phosphates, and carbonates. *Sci. Adv.* **4**, eaao6250 (2018).
34. K. Them, F. Ellermann, A. N. Pravdivtsev, O. G. Salnikov, I. V. Skovpin, I. V. Koptyug, R. Herges, J. B. Hövener, Parahydrogen-induced polarization relayed via proton exchange. *J. Am. Chem. Soc.* **143**, 13694–13700 (2021).
35. S. Alcicek, P. Put, D. Barskiy, V. Kontul, S. Pustelny, Zero-field NMR of urea: Spin-topology engineering by chemical exchange. *J. Phys. Chem. Lett.* **12**, 10671–10676 (2021).
36. S. Knecht, J. W. Blanchard, D. Barskiy, E. Cavallari, L. Dagys, E. Van Dyke, M. Tsukanov, B. Bliemel, K. Münnemann, S. Aime, F. Reineri, M. H. Levitt, G. Buntkowsky, A. Pines, P. Blümler, D. Budker, J. Eills, Rapid hyperpolarization and purification of the metabolite fumarate in aqueous solution. *Proc. Natl. Acad. Sci. U.S.A* **118**, 2025383118 (2021).
37. D. M. Doddrell, D. T. Pegg, M. R. Bendall, Distortionless enhancement of NMR signals by polarization transfer. *J. Magn. Reson.* **48**, 323–327 (1982).
38. T. F. Sjolander, J. W. Blanchard, D. Budker, A. Pines, Two-dimensional single- and multiple-quantum correlation spectroscopy in zero-field nuclear magnetic resonance. *J. Magn. Reson.* **318**, 106781 (2020).
39. F. Ruiz, V. Gomis, R. F. Botella, Extraction of ethanol from aqueous solution. 2. A solvent more volatile than ethanol: Dichloromethane. *Ind. Eng. Chem. Res.* **27**, 648–650 (1988).

40. A. H. Trabesinger, R. McDermott, S. Lee, M. Mück, J. Clarke, A. Pines, SQUID-detected liquid state NMR in microtesla fields. *J. Phys. Chem. A* **108**, 957–963 (2004).
41. F. Verpillat, M. P. Ledbetter, S. Xu, D. J. Michalak, C. Hilty, L.-S. Bouchard, S. Antonijevic, D. Budker, A. Pines, Remote detection of nuclear magnetic resonance with an anisotropic magnetoresistive sensor. *Proc. Natl. Acad. Sci.* **105**, 2271–2273 (2008).
42. H. Zheng, J. Xu, G. Z. Iwata, T. Lenz, J. Michl, B. Yavkin, K. Nakamura, H. Sumiya, T. Ohshima, J. Isoya, J. Wrachtrup, A. Wickenbrock, D. Budker, Zero-field magnetometry based on nitrogen-vacancy ensembles in diamond. *Phys. Rev. Appl.* **11**, 064068 (2019).
43. B. A. Rodin, K. L. Ivanov, Representation of population exchange at level anti-crossings. *Magn. Reson. Discuss.* **1**, 347–365 (2021).
44. E. B. Dücker, L. T. Kuhn, K. Münnemann, C. Griesinger, Similarity of SABRE field dependence in chemically different substrates. *J. Magn. Reson.* **214**, 159–165 (2012).
45. P. J. Rayner, B. J. Tickner, W. Iali, M. Fekete, A. D. Robinson, S. B. Duckett, Relayed hyperpolarization from para-hydrogen improves the NMR detectability of alcohols. *Chem. Sci.* **10**, 7709–7717 (2019).
46. S. Knecht, D. A. Barskiy, G. Buntkowsky, K. L. Ivanov, Theoretical description of hyperpolarization formation in the SABRE-relay method. *J. Chem. Phys.* **153**, 164106 (2020).
47. M. Emondts, D. Schikowski, J. Klankermayer, P. P. M. Schleker, Non-pairwise interactions in parahydrogen experiments: Nuclear exchange of single protons enables bulk water hyperpolarization. *ChemPhysChem* **19**, 2614–2620 (2018).
48. A. N. Pravdivtsev, K. L. Ivanov, A. V. Yurkovskaya, P. A. Petrov, H. H. Limbach, R. Kaptein, H. M. Vieth, Spin polarization transfer mechanisms of SABRE: A magnetic field dependent study. *J. Magn. Reson.* **261**, 73–82 (2015).
49. I. V. Zhukov, A. S. Kiryutin, Z. Wang, M. Zachrdla, A. V. Yurkovskaya, K. L. Ivanov, F. Ferrage, Surprising absence of strong homonuclear coupling at low magnetic field explored by two-field nuclear magnetic resonance spectroscopy. *Magn. Reson.* **1**, 237–246 (2020).
50. T. R. Eichhorn, A. J. Parker, F. Josten, C. Müller, J. Scheuer, J. M. Steiner, M. Gierse, J. Handwerker, M. Keim, S. Lucas, M. U. Qureshi, A. Marshall, A. Salhov, Y. Quan, J. Binder, K. D. Jahnke, P. Neumann, S. Knecht, J. W. Blanchard, M. B. Plenio, F. Jelezko, L. Emsley, C. C. Vassiliou, P. Hautle, I. Schwartz, Hyperpolarized solution-state NMR spectroscopy with optically polarized crystals. *J. Am. Chem. Soc.* **144**, 2511–2519 (2022).

Acknowledgments: We thank P. Blümler for the construction of the "Barskiy-Eills" magnet capable of providing a variable field in the range of 1 to 101 mT depending on the relative angle between two enclosed Halbach magnets. **Funding:** This work was supported by the Alexander von Humboldt Foundation in the framework of Sofja Kovalevskaja Award, German Research Foundation (DFG) project number 465084791, and European Union's Horizon 2020 research and innovation program under the Marie Skłodowska-Curie grant agreement no. 766402. **Author contributions:** Conceptualization: D.A.B. Methodology: E.T.V.D., J.E., R.P.-F., K.F.S., Y.H., and D.A.B. Investigation: E.T.V.D., J.E., R.P.-F., K.F.S., and D.A.B. Supervision: D.B. and D.A.B. Writing—original draft: E.T.V.D. and D.A.B. Writing—review and editing: E.T.V.D., J.E., R.P.-F., K.F.S., Y.H., D.B., and D.A.B. **Competing interests:** The authors declare that they have no competing interests. **Data and materials availability:** All data needed to evaluate the conclusions in the paper are present in the paper and/or the Supplementary Materials.

Submitted 7 March 2022
Accepted 7 June 2022
Published 20 July 2022
10.1126/sciadv.abp9242